

Drops on an inclined heterogeneous substrate: onset of sliding motion

Uwe Thiele

*Max-Planck-Institut für Physik komplexer Systeme,
Nöthnitzer Str. 38, D-01187 Dresden, Germany*

Edgar Knobloch

Department of Physics, University of California, Berkeley, CA 94720, USA

(Dated: July 12, 2018)

Abstract

Pinning and depinning of drops on an inclined heterogeneous substrate is studied as a function of the inclination and heterogeneity amplitude. Two types of heterogeneity are considered: a hydrophobic defect that blocks the droplet in front, and a hydrophilic one that holds it at the back. Two different types of depinning leading to sliding motion are identified, and the resulting stick-slip motion is studied numerically.

PACS numbers: 47.20.Ky, 47.55.Dz, 68.08.-p, 68.15.+e

It is well known that liquid drops on an ideally smooth substrate move in response to external gradients. For example, a drop on an inclined substrate slides downslope in response to the gradient of potential energy [1, 2]. Likewise a droplet in a temperature gradient will move towards higher temperatures as a result of Marangoni forces caused by surface tension gradients [3]. Alternatively, a wettability gradient induced by a chemical grading of the substrate also causes droplet motion. In order to minimize its energy the droplet will move towards the most wettable region [4, 5]. Although on ideally smooth substrates droplets will move even for arbitrarily small gradients, this is not the case for the 'real' substrates used in experiments. There the onset of contact line motion is strongly influenced by chemical or physical heterogeneities of the substrate and a finite driving force is necessary to overcome the pinning influence of the heterogeneities [6, 7, 8, 9, 10, 11, 12]. On the smaller, atomic scale surface heterogeneities can trap droplets even on very smooth surfaces. Indeed, heterogeneities occurring on a micro- or mesoscale are known to affect the macroscopic movement of droplets and are responsible, for instance, for the observed hysteresis between advancing and receding contact angles [13, 14, 15].

The simplest example of depinning is described by the Adler equation [16]

$$\dot{\theta} = \mu - \sin \theta, \quad (1)$$

where θ represents the position of the droplet, and $\mu > 0$ represents the applied force. When $\mu < 1$ this equation has a pair of fixed points, one of which is stable and the other unstable. At $\mu = 1$ these fixed points annihilate in a saddle-node bifurcation, but unlike the standard saddle-node bifurcation this bifurcation produces periodic motion for $\mu > 1$. This result is simplest to understand if we write Eq. (1) as $\dot{\theta} = -dV/d\theta$, $V \equiv -\mu\theta - \cos \theta$. Evidently, Eq. (1) represents an overdamped particle in a cosinusoidal potential that is progressively tilted as μ increases. A 'particle' in a stable equilibrium at a local minimum of this potential 'spills out' once the tilt becomes large enough that its position no longer corresponds to a minimum. This occurs precisely at $\mu = 1$. The periodic motion present for $\mu > 1$ corresponds to the particle sliding down the resulting 'washboard' potential. The period of this motion diverges as $(\mu - 1)^{-1/2}$ [17]. The resulting bifurcation is sometimes called a Saddle-Node Infinite PERiod bifurcation or 'sniper' for short.

In this paper we explore the process of pinning and depinning of driven droplets on a heterogeneous substrate. For simplicity we consider the case of gravitational forcing on

an inclined substrate with a heterogeneous disjoining potential with a well-defined spatial period such as might arise from spatially varying wetting properties resulting from chemical heterogeneity. This formulation avoids complications arising from changes in surface elevation of the substrate (surface roughness) while retaining the essence of the pinning phenomenon. In addition we focus on nanoscale droplets for which we can solve the governing equation for both the droplet profile and the precursor film, without involving the matched asymptotic expansions required for larger droplets. We avoid energy methods since these do not permit us to study time-dependent phenomena.

A two-dimensional liquid droplet on an inhomogeneous solid substrate subject to a horizontal force μ (Fig.1) is described by an evolution equation for the film thickness profile $h(x, t)$ derived from the Navier-Stokes equation using the long-wave approximation [18]:

$$\partial_t h = -\partial_x \left\{ \frac{h^3}{3\eta} [\partial_x (\gamma \partial_{xx} h + \Pi(h, x)) + \mu] \right\}. \quad (2)$$

Here γ is the surface tension, η is the dynamic viscosity, while $\Pi(h, x)$ is the disjoining pressure that accounts for the wetting properties of the heterogeneous substrate [19]. We use the form $\Pi(h, x) = 2S_a d_0^2/h^3 + (S_p(x)/l) \exp[(d_0 - h)/l]$ [20, 21], where S_a and S_p are the apolar and polar components of the total spreading coefficient $S = S_a + S_p$, $d_0 = 0.158$ nm is the Born repulsion length and l is a correlation length [20], and choose $S_a > 0$ and $S_p < 0$, thereby combining a stabilizing long-range van der Waals liquid-solid interaction with a destabilizing short-range polar interaction. The latter contains the influence of surface coating and wettability defects, and crucially influences the static contact angle [20]. When $\mu = 0$ the resulting model describes static droplets with a finite mesoscopic equilibrium contact angle sitting on an ultrathin precursor film. However, any qualitatively similar disjoining pressure yields like results, as shown for dewetting in [21] and for chemically driven running droplets in [22].

We nondimensionalize Eq. (2) using the scales $3\eta\gamma/\kappa^2 l$ for time, l for the film thickness and $\sqrt{l\gamma/\kappa}$ for the lateral coordinate, where $\kappa = (|S_p|/l) \exp(d_0/l)$. In addition we define the dimensionless quantities $b = (2S_a d_0^2/|S_p|l^2) \exp(-d_0/l)$ and $\alpha = (\gamma l/\kappa^3)^{1/2}(\mu/\rho)$. Thus for gravitational forcing α measures the inclination of the substrate, and we refer to it as the inclination. The loading of the system (relevant for gravitational forcing) is measured by the mean film height $\bar{h} \equiv L^{-1} \int_0^L h(x) dx$.

Figures 2(a,b) show sample steady state profiles for two cases: (a) a hydrophilic defect.

(b) a hydrophobic defect. Both are described by

$$\Pi(h, x) = \frac{b}{h^3} - [1 + \epsilon \xi(x)] e^{-h}, \quad (3)$$

with

$$\xi(x) = \{2 \operatorname{cn}[2K(k)x/L, k]\}^2 - \Delta, \quad (4)$$

where $K(k)$ is the complete elliptic integral of the first kind and Δ is such that the average of $\xi(x)$ over a spatial period vanishes. We use the logarithmic measure $s \equiv -\log(1 - k)$ to quantify the steepness of the heterogeneity profiles (Fig. 2(a,b)). These correspond to hydrophilic ($\epsilon < 0$) or hydrophobic ($\epsilon > 0$) defects. In (a) the droplet is held at the back by a hydrophilic defect and develops a prominent shoulder as α increases just prior to depinning. In contrast in (b) the hydrophobic defect blocks the droplet and its profile steepens with increasing α . The profiles at depinning are shaded. Figures 2(c,d) show the advancing and receding mesoscopic contact angles, measured at the inflection points of the drop profile, as a function of α . For a droplet pinned at the back (Fig. 2(c)) the advancing [receding] angle decreases [increases] for small but increasing inclination α . However, once the droplet starts developing a shoulder at the back the receding angle decreases again until depinning occurs. The situation differs for a droplet pinned at the front (Fig. 2(d)). In this case both angles increase with α but drop just prior to depinning (Fig. 2).

The depinning process corresponds to the loss of stability of the pinned drop. The stability calculation [23] reveals two mechanisms that lead to depinning. The first is via a sniper bifurcation (i.e., a steady state bifurcation) and prevails for hydrophobic defects with small wettability contrast [23] and for hydrophilic defects. Figure 3(a) shows a typical bifurcation diagram for the latter case as a function of increasing α . The figure shows the L^2 norm of $\delta h \equiv h(x) - \bar{h}$ for pinned drops and its time-average after depinning. Although there are two saddle-node bifurcations in the diagram time integration (open circles) shows that the upper part of the branch of pinned drops is stable until the rightmost saddle-node bifurcation. Thereafter the solutions are time-dependent but periodic (open triangles). The inset shows that near the saddle-node the period diverges like $(\alpha - \alpha_c)^{-1/2}$ and hence that in this case depinning corresponds to a sniper bifurcation. Figures 3(b,c) show space-time plots of the resulting motion for (b) $\alpha \gtrsim \alpha_c$, and (c) $\alpha = 0.04$. In (b) the drop spends a long time in a nearly stationary state while slowly spreading downstream, before it abruptly breaks off and moves towards the next defect. In contrast in (c) the drop flows more or

less at constant speed downslope, although the location of the defect remains visible in the space-time plot.

Figure 4(a) shows the location of the two saddle-nodes in the (ϵ, α) plane. In the case of a hydrophilic defect ($\epsilon < 0$) the saddle-nodes are always present; the one at larger α corresponds to the depinning bifurcation. For fixed \bar{h} and large L the critical α decreases as $1/L$ (not shown), as expected on the basis of simple loading ideas. However, the figure also shows that something else happens for sufficiently hydrophobic defects. Here the saddle-nodes annihilate at $\epsilon \approx 0.6$, and depinning now occurs via a Hopf bifurcation (dashed line). The resulting bifurcation diagram (Fig. 5(a)) shows that the range of stable pinned profiles overlaps with the range of periodic states generated by the instability. Thus in this case the branch of periodic solutions loses stability at a saddle-node bifurcation as α decreases, and the system settles into a steady pinned state in a hysteretic transition. Figures 5(b,c) show space-time plots of the periodic state near this transition and further away. Here the depinning is as abrupt as in Fig. 3(b) but without the slow downstream leakage seen in the latter figure. The resulting dynamics strongly resemble stick-slip motion. However, further away from the transition the depinned states in both cases look quite alike: in both cases the droplet travels at almost constant speed, only slightly modulated by the heterogeneity.

The advancing and receding angles at depinning (shaded profiles in Fig. 2) shown in Fig. 4(b) provide a measure of the contact angle hysteresis observed macroscopically. In the case of a hydrophobic defect at the front ($\epsilon > 0$) both angles increase nearly linearly with defect strength, and continue to do so even for oscillatory depinning ($\epsilon \gtrsim 0.6$); the small hook visible in the figure near this transition indicates that the Hopf bifurcation sets in prior to the disappearance of the saddle-node bifurcations. The behavior is more intricate when the pinning is by a hydrophilic defect at the back ($\epsilon < 0$). In this case the role of the two angles is reversed, and both decrease nearly linearly with slopes identical to those in the $\epsilon > 0$ case. For $\epsilon < -0.2$, however, the receding angle reverses tendency and starts to increase again, while the advancing angle continues to decrease. This change in behavior is a consequence of the stretching of the drop with increasing inclination just prior to depinning: for $\epsilon \lesssim -0.2$ gravity drags the main body of liquid downstream (to the right) but the spot of higher wettability traps part of it upstream. For fixed α the latter effect becomes more pronounced as $|\epsilon|$ increases, cf. Fig. 4(b).

We have examined two types of pinning: pinning by a hydrophilic defect at the back of the

droplet, and pinning by a hydrophobic defect in front of it, and identified two mechanisms whereby pinning takes place. In the case of a sufficiently large hydrophilic defect the droplet stretches markedly just prior to depinning as the substrate inclination increases; the inclined droplet loses stability at a saddle-node bifurcation, resulting in periodic motion as the droplet slides over a periodic array of hydrophilic defects. We have referred to this type of bifurcation as the 'sniper'. The periodic motion that results is slow when the droplet is stretching, and fast once the droplet breaks away from a defect and spills onto the next one. The situation is richer for hydrophobic defects that pin the droplet by blocking it. In this case in addition to the steady state sniper bifurcation a new depinning mechanism was observed: the droplet loses stability to an oscillatory mode prior to depinning. A mode of this type cannot be identified by standard energy arguments. In the example shown this bifurcation is hysteretic. The two depinning scenarios are distinguished primarily by the average speed of the droplet near the depinning transition. In the sniper scenario this speed vanishes as $(\alpha - \alpha_c)^{1/2}$; in the latter it is finite. At larger values of α both scenarios lead to broadly similar dynamics: more-or-less uniform sliding motion modulated by passage over defects. It is noteworthy that no Hopf bifurcation occurs when the wettability profile is sinusoidal [23].

Many depinning phenomena in physics may be understood using the sniper scenario. Usually this is so in systems with a continuous symmetry such as invariance under translations. In the absence of a heterogeneity spatially periodic structures may undergo a spontaneous parity-breaking bifurcation that breaks the left-right symmetry of the pattern and produces a drift. The direction of the drift is then determined by the associated tilt of the structure [24]. In this case the drift speed of the structure vanishes as the square root of the distance from the parity-breaking bifurcation. However, in the presence of spatial heterogeneities the situation changes dramatically because near the bifurcation even small amplitude heterogeneities suffice to pin the tilted structure. A detailed study of this regime [25] shows that while some depinning events are indeed analogous to the behavior described by the Adler equation, a quite different depinning mechanism is present as well. Here the tilted state first undergoes a Hopf bifurcation that produces back-and-forth rocking motion of the tilted structure, but no net translation. As a parameter increases the amplitude of this oscillation increases leading to a global bifurcation involving an unstable fixed point and its translate by one period. This bifurcation generates oscillations with a nonzero mean drift, and this net drift increases with further increase in the parameter. The present system differs in the

absence of left-right symmetry, but a global bifurcation that changes the topology of the limit cycle produced in the Hopf bifurcation from a libration to a rotation must still take place. Such a bifurcation can occur if the Hopf bifurcation is in fact supercritical. Consistency with the Fig. 5(a) requires that the branch of periodic states must go through a pair of saddle-node bifurcations to produce stable states of the type shown in Fig. 5(b).

This work was supported by NASA, NSF and EU under grants NNC04GA47G (EK,UT), DMS-0305968 (EK) and MRTN-CT-2004-005728 (UT).

-
- [1] T. Podgorski, J.-M. Flesselles, and L. Limat, *Phys. Rev. Lett.* **87**, 036102 (2001).
 - [2] U. Thiele, M. G. Velarde, K. Neuffer, M. Bestehorn, and Y. Pomeau, *Phys. Rev. E* **64**, 061601 (2001).
 - [3] F. Brochard, *Langmuir* **5**, 432 (1989).
 - [4] E. Raphaël, *C. R. Acad. Sci. Ser. II* **306**, 751 (1988).
 - [5] M. K. Chaudhury and G. M. Whitesides, *Science* **256**, 1539 (1992).
 - [6] L. W. Schwartz and S. Garoff, *Langmuir* **1**, 219 (1985).
 - [7] G. D. Nadkarni and S. Garoff, *Langmuir* **10**, 1618 (1994).
 - [8] A. Marmur, *Colloid Surf. A-Physicochem. Eng. Asp.* **116**, 55 (1996).
 - [9] D. Quéré, M. J. Azzopardi, and L. Delattre, *Langmuir* **14**, 2213 (1998).
 - [10] E. Schäffer and P. Z. Wong, *Phys. Rev. E* **61**, 5257 (2000).
 - [11] P. Roura and J. Fort, *Phys. Rev. E* **64**, 011601 (2001).
 - [12] U. Thiele, L. Bruschi, M. Bestehorn, and M. Bär, *Eur. Phys. J. E* **11**, 255 (2003).
 - [13] E. B. Dussan, *Ann. Rev. Fluid Mech.* **11**, 371 (1979).
 - [14] P.-G. de Gennes, *Rev. Mod. Phys.* **57**, 827 (1985).
 - [15] L. Leger and J. F. Joanny, *Rep. Prog. Phys.* **55**, 431 (1992).
 - [16] R. Adler, *Proc. I.R.E. Waves Electrons* **34**, 351 (1946).
 - [17] S. H. Strogatz, *Nonlinear Dynamics and Chaos* (Addison-Wesley, 1994).
 - [18] A. Oron, S. H. Davis, and S. G. Bankoff, *Rev. Mod. Phys.* **69**, 931 (1997).
 - [19] J. N. Israelachvili, *Intermolecular and Surface Forces* (Academic Press, London, 1992).
 - [20] A. Sharma, *Langmuir* **9**, 861 (1993).
 - [21] U. Thiele, K. Neuffer, Y. Pomeau, and M. G. Velarde, *Colloid Surf. A* **206**, 135 (2002).

- [22] K. John, M. Bär, and U. Thiele, *Eur. Phys. J. E* **18**, 183 (2005).
- [23] U. Thiele and E. Knobloch, preprint (2006).
- [24] P. Coullet, R. E. Goldstein, and G. H. Gunaratne, *Phys. Rev. Lett.* **63**, 1954 (1989).
- [25] G. Dangelmayr, J. Hettel, and E. Knobloch, *Nonlinearity* **10**, 1093 (1997).

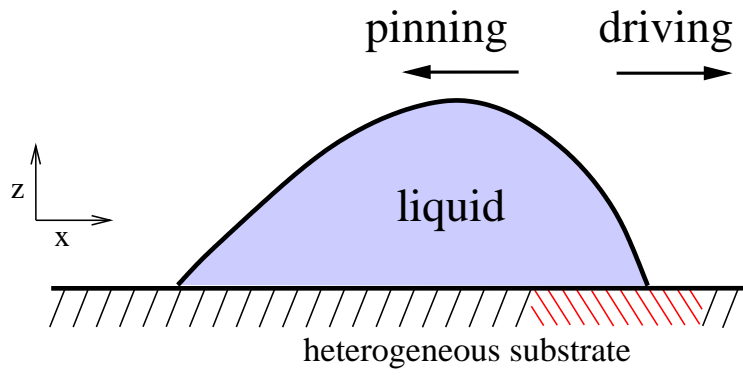


FIG. 1: Sketch of a droplet on a heterogeneous substrate subject to a horizontal force μ towards the right.

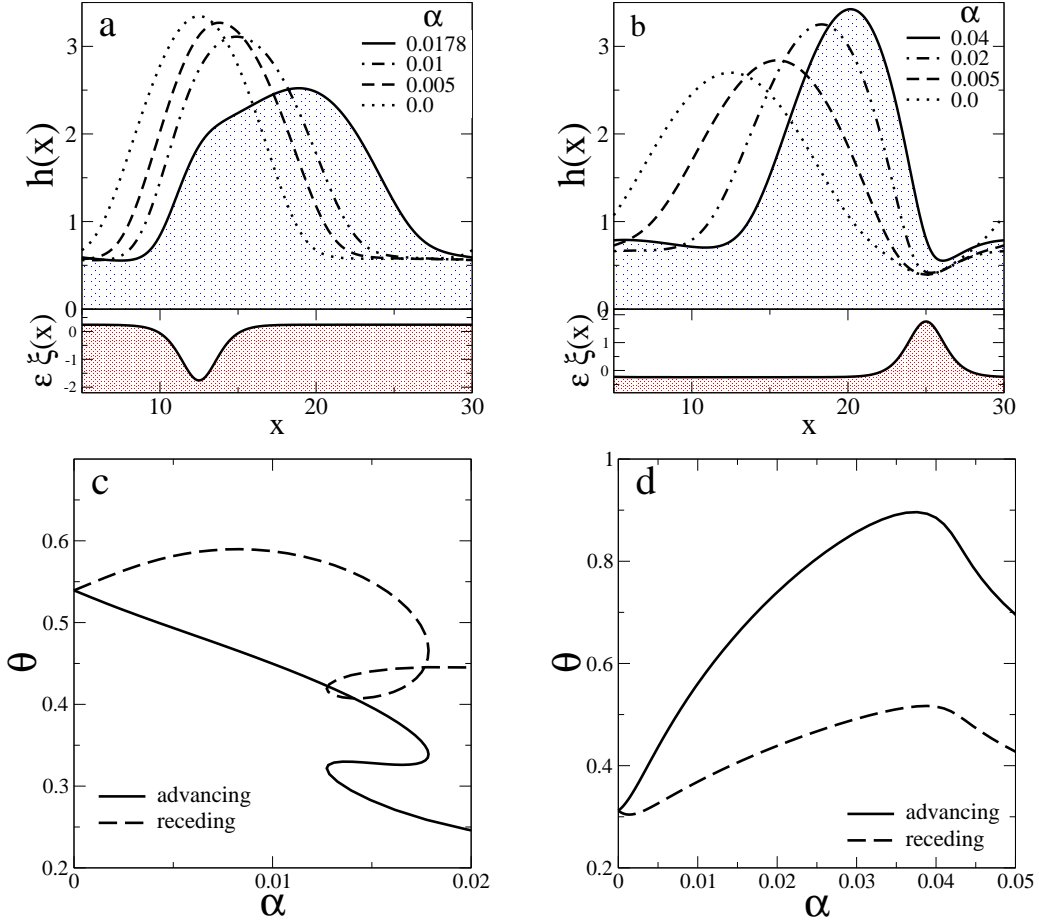


FIG. 2: Characteristics of pinned droplets as a function of the forcing α for localized hydrophilic [(a) and (c), $\epsilon = -1$] and hydrophobic [(b) and (d), $\epsilon = 1$] defects. The upper parts of (a) and (b) show steady droplet profiles while the lower parts show the wettability profile [Eq. (4) with $s = 6$]. The profile at depinning is shaded. In (a) the droplet is pinned by a more wettable defect at the back whereas in (b) it is blocked by a less wettable defect in front. Panels (c) and (d) show the advancing and receding contact angles θ as a function of α . The remaining parameters are $L = 25$, $b = 0.1$, and $\bar{h} = 1.5$.

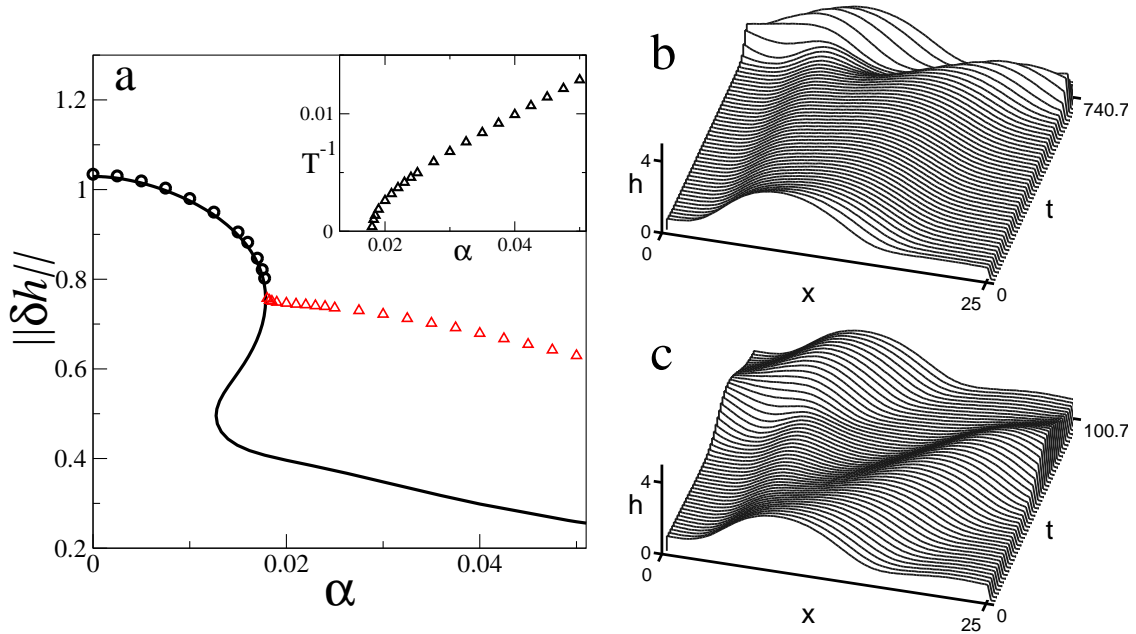


FIG. 3: (a) Bifurcation diagram for depinning via a sniper bifurcation for a hydrophilic defect [Eq. (4) with $s = 6$] with $\epsilon = -1.0$ and $L = 25$, $b = 0.1$, $\bar{h} = 1.5$. The figure shows the L^2 -norm of steady solutions (solid line), selected steady solutions as obtained by integration in time (circles) and the time-averaged L_2 -norm for the unsteady solutions beyond depinning (triangles). Inset shows the inverse of the temporal period T for the latter. The remaining panels show space-time plots over one spatial and temporal period for a sliding drop (b) close to depinning at $\alpha = 0.0185$ with $T = 556.1$, and (c) far from depinning at $\alpha = 0.04$ with $T = 100.7$.

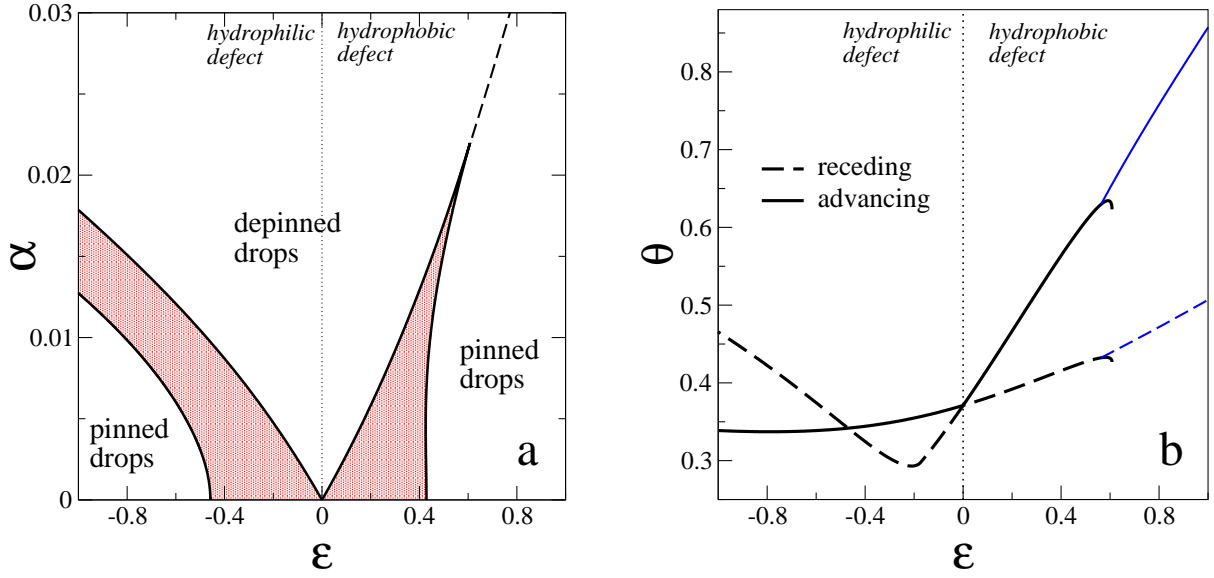


FIG. 4: (a) Phase diagram for the depinning transition for localized hydrophilic ($\epsilon < 0$) or hydrophobic ($\epsilon > 0$) defects [Eq. (4) with $s = 6$]. The figure focuses on small wettability contrast and $L = 25$, $b = 0.1$, $\bar{h} = 1.5$. The solid [dashed] lines correspond to saddle-node [Hopf] bifurcations. The latter emerge near the cusp at which the two saddle-node bifurcations annihilate for $\epsilon > 0$. (b) Advancing (solid lines) and receding (broken lines) contact angles θ at the depinning transition as a function of wettability contrast for a hydrophilic defect at the back ($\epsilon < 0$) and hydrophobic defect at the front ($\epsilon > 0$). Thick [thin] lines refer to depinning through a real [oscillatory] mode.

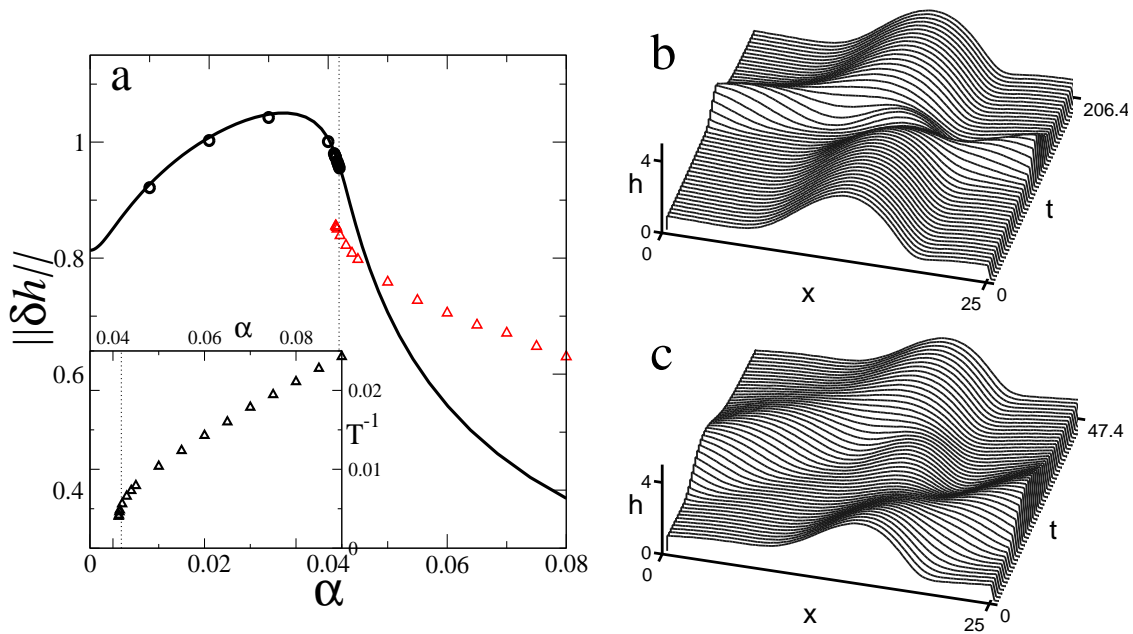


FIG. 5: As for Fig. 3 but showing depinning via a Hopf bifurcation when $\epsilon = 1.0$. (a) Bifurcation diagram. (b) Space-time plot for $\alpha = 0.0415$ with $T = 206.4$. (c) $\alpha = 0.08$ with $T = 47.4$. The vertical line indicates the location of the Hopf bifurcation as obtained from linear stability theory [23].